Driving CO_2 to a Quasi-Condensed Phase at the Interface between a Nanoparticle Surface and a Metal-Organic Framework at 1 bar and 298 K

Hiang Kwee Lee,[1,2] Yih Hong Lee,[1] Joseph V. Morabito,[3] Yejing Liu,[1] Charlynn Sher Lin Koh,[1] In Yee Phang,[2] Srikanth Pedireddy,[1] Xuemei Han,[1] Lien-Yang Chou,[4] Chia-Kuang Tsung,[3,*] Xing Yi Ling[1,*]

[1] Division of Chemistry and Biological Chemistry, School of Physical and Mathematical Sciences, Nanyang Technological University, 21 Nanyang Link, Singapore 637371.

[2] Institute of Materials Research and Engineering, A*STAR (Agency for Science, Technology and Research), 2 Fusionopolis Way, Innovis, #08-03, Singapore 138634.

[3] Department of Chemistry, Merkert Chemistry Center, Boston College, Chestnut Hill, Massachusetts 02467, United States.

[4] School of Physical Science and Technology, ShanghaiTech University, Shanghai 201210, China

KEYWORDS. metal-organic framework, solid-gas, high pressure, ambient operation, surface-enhanced Raman scattering (SERS), carbon dioxide

ABSTRACT: We demonstrate a molecular-level observation of driving CO_2 molecules into a quasi-condensed phase on the solid surface of metal nanoparticles (NP) under ambient conditions of 1 bar and 298 K. This is achieved via a CO_2 accumulation in the interface between a metal-organic framework (MOF) and a metal NP surface formed by coating NPs with a MOF. Using real-time surface-enhanced Raman scattering spectroscopy, a >18-fold enhancement of surface coverage of CO_2 is observed at the interface. The high surface concentration leads CO_2 molecules to be in close proximity with the probe molecules on the metal surface (4-methylbenzenethiol), and transforms CO_2 molecules into a bent conformation without the formation of chemical bonds. Such linear-to-bent transition of CO_2 is unprecedented at ambient conditions in the absence of chemical bond formation, and is commonly observed only at pressurized systems (>10^5 bar). The molecular-level observation of a quasi-condensed phase induced by MOF coating could impact the future design of hybrid materials in diverse applications, including catalytic CO_2 conversion and ambient solid-gas operation.

INTRODUCTION

Collisions between gas molecules and solid surfaces are key steps in all solid-gas processes such as heterogeneous catalysis and molecular sensing.[1, 2] Conventionally, higher collision rates require large energy input, which are usually achieved by increasing the pressure or temperature of the system.[3, 4] An alternative approach to mitigate this energy demand is to enrich the local concentration of gas molecules on solid surfaces, efficiently boosting the collision rates and interaction strength at the point-of-use while allowing the system to remain at ambient pressure and temperature. Metal-organic frameworks (MOFs) are one of the most powerful material to accumulate and enrich gases with molecular specificity; therefore, covering solid surfaces with MOFs holds promise in enriching target gas molecules at surfaces.[5-7] Despite the vast potential of solid-MOF interfaces to accumulate gas at the solid surface,[8-10] their exploitation to expedite ambient-operated surface applications is limited owing to a lack of molecular-level understanding of the MOF-induced enrichment process specifically at the solid-MOF interface. Conventional sorption characterization method cannot retrieve real-time molecular information *in situ*.[5, 9, 11] Molecule-specific spectroscopic techniques could be used to characterize MOF-gas interactions in bulk MOF but not molecular-level events occurring at the solid surfaces.[12]

Herein, we used real time surface-enhanced Raman scattering (SERS) spectroscopy to elucidate the molecular dynamics of CO_2 molecules at a designed model solid-MOF interface during gas infusion. Our model solid-MOF interface comprises a zeolitic imidazolate framework-8 (ZIF-8) deposited over an array of Ag nanocubes grafted with surface probe molecules, 4-methylbenzenethiol (MBT). In this model solid-MOF system (Ag@ZIF-8), ZIF-8 provides CO_2 sorption, plasmonic-active Ag nanocubes provide a solid surface and SERS sensitivity, and surface-grafted MBT functions as a spectroscopic probe to track molecular-level changes near the solid surface.[13] For the first time, we demonstrate the enrichment of target gas molecules, CO_2, at the solid-MOF interface at 1 bar and 298 K without the

formation of chemical bond. The >18-fold enhancement of surface coverage of CO_2 drives gaseous even alters the conformation of CO_2 molecules. Such conformation transformation occurring without involving chemical bond formation is commonly observed only in liquid CO_2 phase and at pressures greater than 10^5 bar.[14] This molecular-level observation of pseudo high-pressure states at the interface provides new insights to previous works, where MOFs were used to enrich gas molecules near solid surface through their sorption within the inherent micropores of MOF.[7, 9] The valuable insights gained in this work therefore further the possibility of promoting the interactions between gas molecules and solid surface at ambient operations, and promise new heterogeneous reaction pathways of catalytic conversions such as CO_2 reduction.

RESULTS AND DISCUSSIONS

We use a wet chemical overgrowth method to prepare our Ag@ZIF-8 platform, depositing ZIF-8 on a Ag nanocube array with MBT as surface functional group (Ag-MBT; edge length ~ 121 nm; Figures 1A, 1B, S1).[15] The MBT on Ag surfaces functions as a spectroscopic probe to track molecular events occurring at the interface (Figure 1C). These aromatic moieties generate intense SERS peaks which can vary systematically with changes in its chemical environment especially upon its π-interaction with the quadrupole moment of CO_2.[16, 17] ZIF-8 nucleates on both Ag nanocubes and the supporting Si platform, eventually thickening into a continuous polycrystalline ZIF-8 thin film (thickness = 366 ± 50 nm) that completely covers the Ag nanocube array (Figures 1B, 1D, S2–S6).

The XPS binding energies and SERS vibrational energies from Ag-MBT before and after ZIF-8 formation reveals that there is no direct contact between ZIF-8 and Ag (Figures 1E, 1F, S7-S9). This is probably due to the MBT layers. ZIF-8's intrinsic SERS features are also absent and is likely due to both the separation of ZIF-8 from Ag surfaces, as well as the reduced polarizabilities of 2-methylimidazolate and Zn^{2+} constituents in a rigid crystalline coordination network (Figure S10).[18] Correspondingly, the deposition of ZIF-8 atop of Ag-MBT surface is expected to have molecular-scale interfacial cavities between Ag and the ZIF-8 (Figure 1D),[19-21] which is challenging to be observed by electron microscopy.[19] Simulation studies have shown that gas molecules can be physically accumulated in these completely embedded cavities owing to the rapid decrease of free energy at the geometry-specific fluid interface during continuous gas sorption.[22-24]

To probe the dynamic interaction of CO_2 at the solid-MOF interface, we monitor the on-site and ultrasensitive SERS responses of Ag@ZIF-8 under continuous CO_2 flow (Figure 2A). The SERS spectra are tracked *in situ* from the same spot to accurately reveal the molecular-level changes are solely due to CO_2 infusion. Ag@ZIF-8 is first thermally activated under vacuum and then placed under controlled CO_2 flow (50 sccm) in a sealed cell for temporal SERS experiments. Consistent XRD patterns, film thicknesses, size and morphology of MBT-grafted Ag nanocubes as well as their vibrational signatures affirm that both the structural and chemical integrities of Ag@ZIF-8 are maintained after thermal activation (Figures S4-S6, S11).

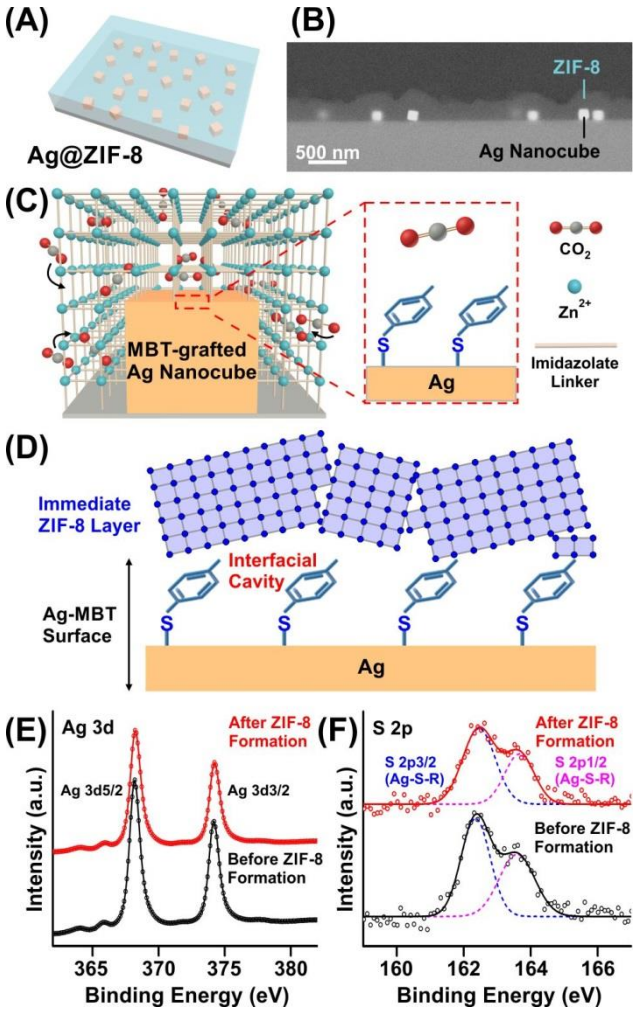

Figure 1. Construction and characterization of Ag@ZIF-8. (A, B) Scheme and cross-sectional SEM image of MBT-grafted Ag nanocube array encapsulated with a film of polycrystalline ZIF-8, respectively. (C) The cavities created at the interface between ZIF-8 and solid surface during Ag@ZIF-8 fabrication. These cavities enable the accumulation of CO_2 molecules on the enclosed solid surface. (D) Proposed overgrowth of polycrystalline ZIF-8 film atop of MBT-grafted Ag nanocube surfaces and the consequential formation of interfacial cavities between Ag and immediate ZIF-8 layer. (E) Ag 3d and (F) S 2p XPS spectra of MBT-grafted Ag nanocubes, both before and after ZIF-8 formation.

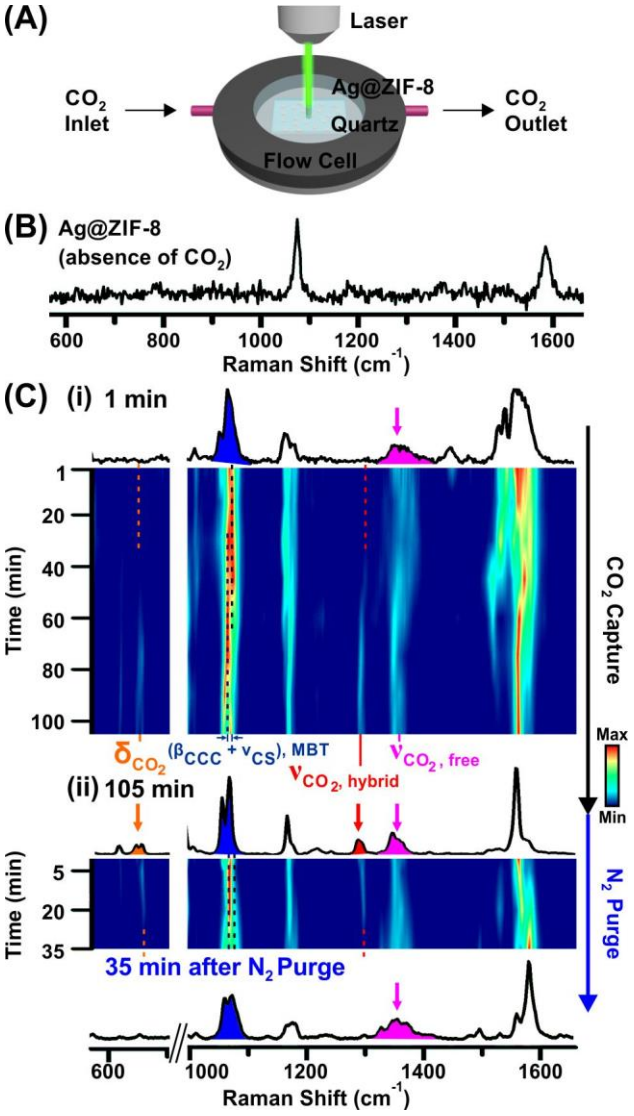

Figure 2. Real-time tracking of spectral evolutions directly at the enclosed solid surface in Ag@ZIF-8 during gas infusion. (A) Experimental setup for *in situ* SERS monitoring of CO_2 capture by Ag@ZIF-8. (B) SERS spectrum of Ag@ZIF-8 in the absence of CO_2 flow. (C) Time-resolved SERS spectra recorded from Ag@ZIF-8 (i) under continuous CO_2 flow for 105 min, and (ii) subsequent purging using N_2 gas for 35 min. The colored regions are of interest for later elucidation of temporal solid-gas dynamics. All gas flow rates are controlled at 50 sccm using mass flow controller and Ag@ZIF-8 is pre-activated at 120 °C under vacuum for 2 h.

A unique spectral evolution is observed throughout the time-dependent SERS studies (Figures 2B, 2C). The initial SERS spectrum of Ag@ZIF-8 in the absence of CO_2 flow exhibits only MBT's characteristic vibrational modes involving a combination of benzene ring breathing mode and C-S stretching mode ($\beta_{CCC} + \nu_{CS}$) at 1075 cm^{-1}, as well as phenyl stretching at 1583 cm^{-1} (Figure 2B).[25, 26] Upon 1 min of CO_2 flow, a new broad band emerges at ~ 1365 cm^{-1} (Figures 2C-i, S12, S13), which gradually narrows over prolonged CO_2 exposure until 105 min. At 45 min, we also note the appearance of two distinct SERS signatures at 653 cm^{-1} and 1299 cm^{-1}. The 1299 cm^{-1} vibrational mode subsequently experiences a ~ 10 cm^{-1} red-shift to 1289 cm^{-1} on further CO_2 sorption by Ag@ZIF-8 until 105 min. This is also accompanied by the progressive red-shifting of MBT's ($\beta_{CCC} + \nu_{CS}$) from ~ 1075 cm^{-1} to 1063 cm^{-1}. More importantly, changes in these SERS spectral features are reverted upon subsequent flushing of the flow cell with nitrogen gas (Figures 2C-ii, S12); the 1365 cm^{-1} signal returns to its original broad feature, SERS bands at 1289 cm^{-1} and 653 cm^{-1} diminish, MBT's ($\beta_{CCC} + \nu_{CS}$) reverts from 1063 cm^{-1} to initial 1075 cm^{-1}. On the contrary, Ag@ZIF-8 under N_2 flow shows no spectral changes (Figures 3A, 3B, S14), thus excluding the possibility of spectral changes arising from laser-induced processes within Ag@ZIF-8. Collectively, the spectral evolutions reveal the quick reversibility of the interactions, which indicates that there is no formation of chemical bonds during the process.[27] This is reasonable because CO_2 adsorbs weakly even on clean Ag surfaces.[28] Potential influence of bulk MOF-CO_2 interaction on the recorded spectra is also negligible as SERS evaluations only reflect the environment immediate to the solid surface. This is further supported by the lack of ZIF-8's intrinsic SERS features, as well as the notable concurrent alteration of surface-grafted MBT's vibrational modes when new SERS bands at 653 cm^{-1} and 1299 cm^{-1} emerged at $t \geq 45$ min; that is, CO_2 molecules have to be near the Ag surface to cause a change in the vibrational energies of surface-grafted MBT molecules.

Controlled experiments were performed over two different platforms including Ag-MBT without ZIF-8 and Ag-MBT drop-casted with pre-formed ZIF-8 nanoparticles (Figures 3C,D). The spectral transformations observed in Ag@ZIF-8 under identical experimental conditions are not observed/sustained in the two control set-ups (Figures 3C, 3D, S15, S16). These comparisons ascertain the continuous accumulation of CO_2 in the interfacial cavity as the driving force behind the spectral transformations, which is only possible upon the complete encapsulation of Ag-MBT surfaces using a ZIF-8 overgrowth layer. It is worth mentioning that the lack of SERS transformations in the absence of ZIF-8 (Figure 3D) again reveals that the temporal vibrational responses using Ag@ZIF-8 are not due to the chemical bonding between CO_2 and Ag.

To identify the molecular origin of the SERS spectral features recorded at the interface, we employ density functional theory (DFT) to examine Ag-MBT and CO_2 interactions and their corresponding simulated SERS spectra. r is defined as the intermolecular separation between the C atom of CO_2 and C_2 of MBT (Figure 4A). Intermolecular separation is systematically varied to simulate the effect of increasing CO_2 concentration in the interfacial cavities, which is expected to force gas molecules towards the surface MBT.[29, 30] This study mainly focuses on the surface interactions as they are directly relevant to our surface-sensitive SERS experiment. CO_2 in the bulk ZIF-8 during gas sorption are excluded from the simulation. The solid surface is represented by an ensemble of MBT molecule on the apex of a Ag_6 cluster (Ag-MBT). We place a CO_2 molecule near Ag-MBT and the system is then allowed to relax. An energetically optimized configuration is achieved at r = 3.7 Å (Figure 4B), characterized as $\Delta E = 0$ kJ/mol. Assuming that the accumulation of CO_2 molecules on the solid surface during the experiments will force some CO2 molecules to move toward Ag-MBT, we gradually reduced r and simulated the energy-favorable configurations and the associated SERS spectra. The simulated results indicate that CO_2 preferably approaches Ag-MBT near MBT's C2 position due to the reduced steric repulsion as compared to neighboring carbon atoms (Figure S17). Also, as a CO_2 molecule is forced to approach the Ag-MBT, the linear CO_2 altered to a bent structure to reduce steric repulsion and

minimize the overall Gibbs energy ($r \leq 3$ Å; Figures 4A, 4B).[14, 31] The required energy for the structural changes is likely compensated by the exothermic adsorption of CO_2 in ZIF-8.[23, 24] More importantly, the simulated spectra of the structural conformation convolution fits our experimental observation. We will elaborate our discussion in the following parts.

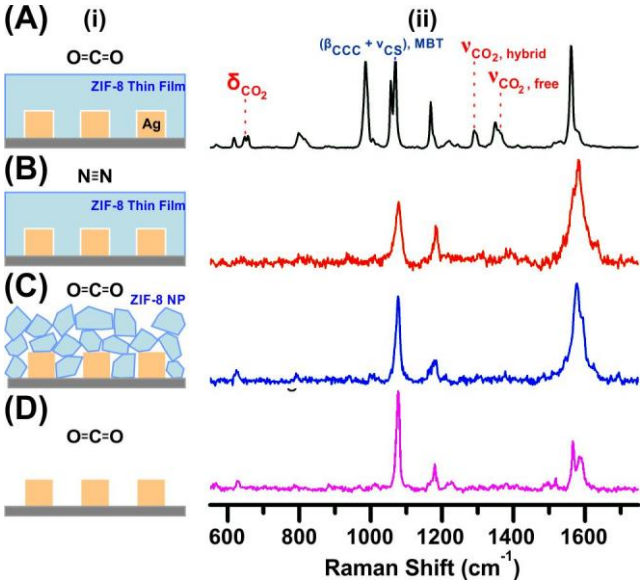

Figure 3. Affirming the continuous accumulation of CO_2 in Ag@ZIF-8 as the driving force behind its spectral transformations. Comparison of SERS evolution across different experimental conditions including (A) Ag@ZIF-8 under CO_2 flow, (B) Ag@ZIF-8 under N_2 flow, (C) Ag-MBT array with a drop-cast (not overgrown) layer of ZIF-8 nanoparticles (ZIF-8 NP) under CO_2 flow, and (D) Ag-MBT array under CO_2 flow. (i, ii) Schematic illustration of various platforms and their corresponding SERS/Raman spectra, respectively. All platforms are pre-activated at 120 °C under vacuum for 2 h. SERS spectra (A – D) are recorded at 105 min after respective gas flow at 50 sccm.

Symmetry-related selection rules of SERS enable us to visualize the *in situ* linear-to-bent transformation of CO_2 at the solid-gas interface with increased gas accumulation over time. Linear CO_2 (point group = $D_{\infty h}$) has a Raman-inactive bending mode because there is no change in polarizability for this molecular vibration.[14] In contrast, this bending becomes Raman-active for a bent CO_2 conformation (point group = C_{2v}). Indeed, we note the emergent of a SERS band at ~ 653 cm^{-1} (t > 45 min) and index it to the ν_2 CO_2 bending mode (Figures 4C, S12, S18, S19), which is a clear indication on the existence of geometrically bent CO_2 structure. This SERS band therefore provides the first spectroscopic indication of the linear-to-bent transformation of CO_2 molecule at the solid surface- under ambient operations, with resultant bond angle approximating 148°. Such bent molecular geometry is traditionally attained in the quasi-liquid CO_2 phase formed under extreme operational pressure (> 10^5 bar) and temperature (> 500 K) in the absence of MOF.[14] It is also noteworthy that the bending of CO_2 molecules in similar two-molecule system without chemical transformations has also been observed using non-reacting CO_2-benzene mixture under pressurized (> 60 bar) and heated (313 K) conditions. These comparisons evidently denote the pseudo high-pressure microenvironment localized at the enclosed surface of our Ag@ZIF-8 system.[32] Hereafter, we term the intermolecular systems involving linear CO_2 and bent CO_2 as "free" and "hybrid", respectively, according to their independent (former) or synchronous (latter) vibrations with Ag-MBT (Figure S19).

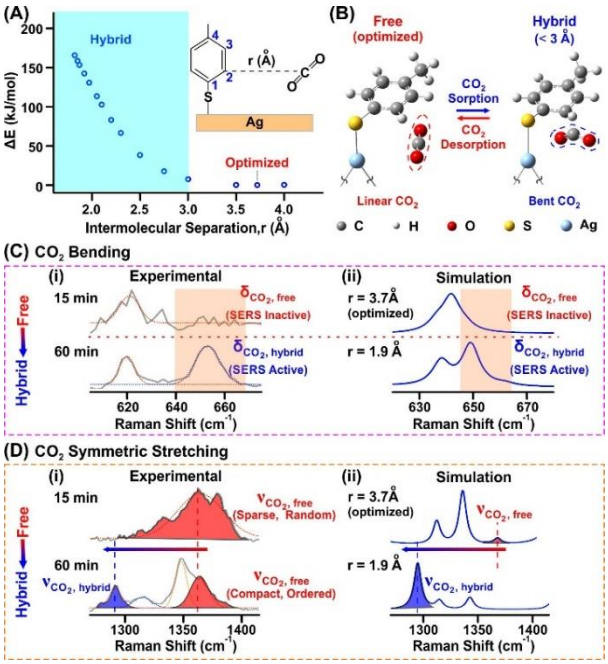

Figure 4. Deciphering the SERS spectral evolutions to unravel the molecular events occurring at the enclosed solid surface of Ag@ZIF-8 system during gas infusion. (A) Variation of molecular system energy with Ag-MBT and CO_2 intermolecular separation. The optimized state (lowest molecular energy) occurs at an intermolecular separation (r) of 3.7 Å. (B) DFT-simulated molecular configurations of CO_2 and Ag-MBT as r decreases. Free state denotes molecular configurations that have minimal Ag-MBT and CO_2 interactions where CO_2 remains in its ground-state linear form and vibrates independently. Hybrid state denotes enhanced Ag-MBT and CO_2 interactions which causes the bent geometry of CO_2 and also synchronous vibration between Ag-MBT and CO_2. Characteristic spectral evolution of (C) CO_2 bending and (D) CO_2 symmetric stretching. (i) Experimental SERS spectra of corresponding Raman shift regions at 15 and 60 min. (ii) Simulated SERS spectra of corresponding Raman shift regions at intermolecular separation of 3.7 and 1.9 Å. The hybrid red-blue arrows in (D) denotes the transition of CO_2 symmetric stretching from free to hybrid mode. For (C, D), the experimental SERS band (left) at ~ 620 cm^{-1}, 1320 cm^{-1} and 1340 cm^{-1} are indexed to the intrinsic vibrational modes of MBT (right).

To comprehend the chronological molecular events leading to linear-to-bent CO_2 transition occurring at solid-MOF interface, we further examine the continuous changes in linear free CO_2 symmetric stretching band at ~ 1365 cm^{-1} over the course of our experiment (Figures 4D, S19). Initially, fast transport of CO_2 through the ZIF-8 layer leads to the appearance of this peak as early as t = 1 min. CO_2 accumulates sparsely in the interfacial cavities, evidenced by the broad peak at t < 45 min. The initial full width at half maximum (FWHM) of this band is 45 cm^{-1}, implying the overall SERS signal comprises an accumulation of multiple vibrational responses from a wide variation of free CO_2 molecules' chemical environments within the interfacial cavi-

ties.[33] The absence of ZIF-8's vibrational signatures also signifies the free CO_2 molecules detected by SERS are likely in the nanoscale interfacial cavity rather than within the pores of ZIF-8. Sustained exposure of Ag@ZIF-8 to CO_2 flow leads to an increased local CO_2 concentration followed by its subsequent saturation at the interface.[23, 24] Ultimately, a quasi-condensed CO_2 liquid state is formed at the Ag-MBT surface which is verified by the experimental narrowing of 1365 cm^{-1} band to a FWHM of 18 (± 1) cm^{-1} at t = 105 min (Figures 4D, S19). The close packing of free CO_2 against the Ag-MBT subsequently triggers a linear-to-bent transformation of CO_2 molecular conformation, as indicated from the emergence of hybrid CO_2 modes indexed to its bending and symmetric stretching at 653 cm^{-1} and 1299 cm^{-1} (t = 45 min), respectively. The latter vibrational mode also exhibits a systematic lowering of its energy to ~ 1289 cm^{-1} (t = 105 min) which correlates to a reduction of r from ~ 1.9 Å to ~ 1.8 Å based on the simulation (Figure S19). Such red-shifts likely arises from the weakening of the respective bonds due to enhanced steric repulsion and/or stronger intermolecular π interaction at smaller r (Table S1).[17] We also exclude the possibility of SERS bands at ~ 1299 cm^{-1} and 1365 cm^{-1} as Fermi resonance doublets owing to their independent SERS spectral changes (discussed later in Figure S27).

Our hypothesis on the formation of quasi-condensed CO_2 phase is further justified by the concurrent red-shifting of MBT's ($\beta_{CCC} + \nu_{CS}$) mode from 1075 cm^{-1} to ~ 1063 cm^{-1}, both experimentally and using simulation as CO_2 molecules approach Ag-MBT (Figure S17). Various spectral evolutions of other MBT's vibrational modes and CO_2 asymmetric stretching also agree with our proposed solid-gas dynamics (Supporting Information Text S1; Figure S20-S23). While the pin-pointing of intermolecular separation is intrinsically challenging and SERS responses are an average of many molecular conformations, the direct SERS read-out of molecular events enabled by Ag-MBT (Figures S24, S25) clearly documents the gas enrichment process and subsequent advancement of CO_2 molecules towards Ag-MBT. More importantly, our comprehensive investigations reveal valuable insights on the pseudo-pressurized microenvironment confined near the solid surface of solid@MOF ensembles. These findings are therefore a significant progress from previous solid@MOF reports,[7, 9] which commonly assumed the molecular concentrating process as a mere confinement of gas molecules near the solid surface via their sorption in the intrinsic micropores of MOF entity. The elucidation of such complex molecular dynamics in solid@MOF system is crucial to expand the possibility of nanoscale solid-gas activation by creating a localized pressurized state at the point-of-use, with the ultimate goal of achieving energetically-green and efficient heterogeneous processes.

Distributions of free and hybrid CO_2/MBT within the interfacial cavity (Figures 5A, S26) are further reconstructed from the temporal vibrational signatures to provide crucial information pertaining to CO_2 interfacial coverage and composition of metastable bent CO_2 at the interface. Both are key characteristics governing high-performance applications involving solid-gas interactions. This investigation is conducted by monitoring the temporal evolution of free and hybrid SERS bands attributed to both CO_2 symmetric stretching and MBT's ($\beta_{CCC} + \nu_{CS}$). The two vibrational modes are chosen due to their constant and evident transformations with continuous CO_2 flow along with their strong intensities. First, the compositional variation of free CO_2 and hybrid CO_2 along the x-z plane perpendicular to Ag-MBT surfaces (Figures 5A, S26) is compared using their characteristic CO_2 symmetric stretching SERS bands at 1365 cm^{-1} and 1295 cm^{-1}, respectively. The relative SERS contribution (I_{hybrid}/I_{free}) gradually increases from ~ 0.1 at 45 min to ~ 0.7 at 105 min, and is accompanied by the concurrent red-shifting of hybrid CO_2 symmetric stretching energy by ~ 10 cm^{-1} as CO_2 molecules approach Ag-MBT (Figures 5B, S27). As relative SERS contribution is indicative of hybrid-to-free states population,[34] our results therefore demonstrate the continuous MOF-induced concentration of CO_2 near the solid surface to increase the relative composition of hybrid CO_2 by driving the linear-to-bent transformation of CO_2. Ultimately, an equilibrium between ground state linear CO_2 and energetically-uphill bent CO_2 configuration is attained.

Similarly, free and hybrid MBT's ($\beta_{CCC} + \nu_{CS}$) bands at ~ 1075 cm^{-1} and 1063 cm^{-1}, respectively, are quantified to unveil the interfacial coverage of gas molecules along solid surfaces (Figures 5A, S26), a crucial indicator on potential solid-gas collisions to afford high-performance surface-based applications. Temporal SERS evaluation of these two modes reveals that MBT's composition at ≤ 1 min comprises entirely of free MBT (I_{hybrid}/I_{free} = 0; Figures 5C, S27). Hybrid MBT emerges at t = 15 min (I_{hybrid}/I_{free} ~ 0.6) and continue to increase until an eventual relative SERS contribution of ~ 10.8 at 105 min. Slight discrepancies to the apparent onset of hybrid MBT's ($\beta_{CCC} + \nu_{CS}$) stretching and CO_2 symmetric stretching mode (t = 45 min) are probably due to the initial difficulty in distinguishing hybrid CO_2 mode from the broad free CO_2 vibrational band centered at 1365 cm^{-1} (Figure S19). Nevertheless, the comparison of relative SERS contribution of hybrid MBT between t = 15 min and t = 105 min clearly demonstrates a > 18-fold boost in interfacial coverage of solid-gas interaction that is rendered possible via the pseudo high-pressure microenvironment achieved in Ag@ZIF-8.

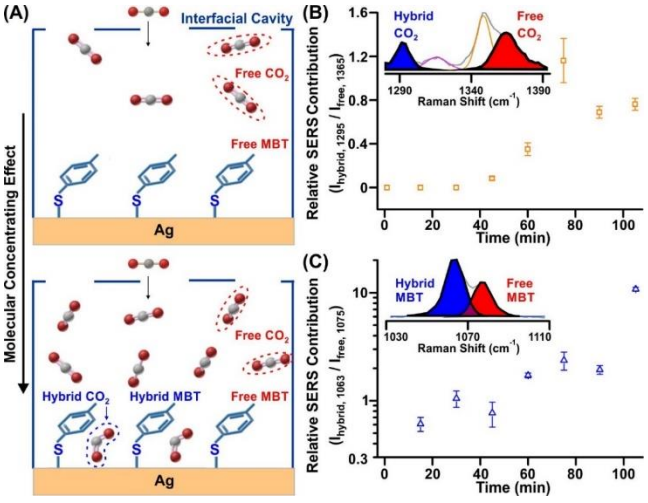

Figure 5. Quantitative reconstruction of the MOF-induced gas enrichment process occurring within the interfacial cavity in a solid@MOF system at ambient operations. (A) Schematic illustration on the utilization of MOF-induced molecular concentrating effect to enhance CO_2 coverage at the solid surfaces, and also promote the transformation of CO_2 molecules into an energetically-elevated bent configuration. Real-time examination on the relative SERS contribution of free and hybrid (B) CO_2 and (C) MBT with increasing CO_2 exposure. Insets of (B) and (C) are the magnified

experimental SERS spectra depicting the deconvoluted free and hybrid SERS bands of CO_2 symmetric stretching and MBT's (β_{CCC} + ν_{CS}), respectively.

CONCLUSION

In summary, our work highlight that MOFs could concentrate CO_2 at the solid surface into a quasi-condensed CO_2 liquid phase even at 1 bar and 298 K. Such condensed phase enforces a wide and > 18-fold increase of surface coverage, as well as the remarkable establishment of a linear-to-bent transformation of CO_2 molecules at the enclosed solid surface even without chemical bond formation. It is also noteworthy that the quasi-condensed CO_2 liquid phase is sustainable in constant CO_2 flow at ambient operations. Our experimental and simulation findings can therefore jointly aid in the rationalizations on the apparent reduction of reaction's activation energy in many previously reported solid-MOF systems.[6, 35, 36] This clearly underscores the importance of pseudo high-pressure microenvironments generated in MOF-encapsulated platforms to realize ideal solid-gas applications by overcoming current operational requirements of immense gas pressure and temperature.

ASSOCIATED CONTENT

Supporting Information. Experimental procedures, figures showing experimental SEM, UV-vis, EDX, XRD, XPS characterizations as well as *in situ* SERS monitoring of Ag@ZIF-8 and other control platforms, figures and table displaying DFT-simulated SERS spectra and molecular configurations. This material is available free of charge via the Internet at http://pubs.acs.org.

AUTHOR INFORMATION

Corresponding Author

* frank.tsung@bc.edu; xyling@ntu.edu.sg

Notes

The authors declare no competing financial interest.

ACKNOWLEDGMENT

X.Y.L. thanks the financial support from National Research Foundation, Singapore (NRF-NRFF2012-04), Nanyang Technological University's start-up grant, and Singapore Ministry of Education, Tier 1 (2016-T1-001-101) and Tier 2 (MOE2016-T2-1-043) grants. H.K.L. appreciates the A*STAR Graduate Scholarship support from A*STAR, Singapore. C.S.L.K. acknowledges support from Nanyang Presidential Graduate Scholarship from Nanyang Technological University. J.V.M. and C.-K.T acknowledge the support from Boston College and the NSF (CHE 1566445).

REFERENCES

1. Yates, J. T.; Campbell, C. T. *Proc. Natl. Acad. Sci. U.S.A.* **2011**, *108*, *911*.
2. Tao, F.; Salmeron, M. *Science* **2011**, *331*, *171*.
3. Somorjai, G. A.; Li, Y. *Proc. Natl. Acad. Sci. U.S.A.* **2011**, *108*, *917*.
4. Schlögl, R. *Angew. Chem. Int. Ed.* **2015**, *54*, *3465*.
5. Wang, B.; Cote, A. P.; Furukawa, H.; O'Keeffe, M.; Yaghi, O. M. *Nature* **2008**, *453*, *207*.
6. Xu, X.; Zhang, Z.; Wang, X. *Adv. Mater.* **2015**, *27*, *5365*.
7. Lu, G.; Li, S.; Guo, Z.; Farha, O. K.; Hauser, B. G.; Qi, X.; Wang, Y.; Wang, X.; Han, S.; Liu, X.; DuChene, J. S.; Zhang, H.; Zhang, Q.; Chen, X.; Ma, J.; Loo, S. C. J.; Wei, W. D.; Yang, Y.; Hupp, J. T.; Huo, F. *Nat. Chem.* **2012**, *4*, *310*.
8. Zhao, M.; Yuan, K.; Wang, Y.; Li, G.; Guo, J.; Gu, L.; Hu, W.; Zhao, H.; Tang, Z. *Nature* **2016**, *539*, *76*.
9. Lu, G.; Farha, O. K.; Kreno, L. E.; Schoenecker, P. M.; Walton, K. S.; Van Duyne, R. P.; Hupp, J. T. *Adv. Mater.* **2011**, *23*, *4449*.
10. Choi, K. M.; Kim, D.; Rungtaweevoranit, B.; Trickett, C. A.; Barmanbek, J. T. D.; Alshammari, A. S.; Yang, P.; Yaghi, O. M. *J. Am. Chem. Soc.* **2017**, *139*, *356*.
11. Chen, Y.-P.; Liu, Y.; Liu, D.; Bosch, M.; Zhou, H.-C. *J. Am. Chem. Soc.* **2015**, *137*, *2919*.
12. Hu, Y.; Liu, Z.; Xu, J.; Huang, Y.; Song, Y. *J. Am. Chem. Soc.* **2013**, *135*, *9287*.
13. Yang, Y.; Lee, Y. H.; Phang, I. Y.; Jiang, R.; Sim, H. Y. F.; Wang, J.; Ling, X. Y. *Nano Lett.* **2016**, *16*, *3872*.
14. Santoro, M.; Gorelli, F. A. *Chem. Soc. Rev.* **2006**, *35*, *918*.
15. Tu, M.; Wannapaiboon, S.; Khaletskaya, K.; Fischer, R. A. *Adv. Funct. Mater.* **2015**, *25*, *4470*.
16. Alba, M.; Pazos-Perez, N.; Vaz, B.; Formentin, P.; Tebbe, M.; Correa-Duarte, M. A.; Granero, P.; Ferré-Borrull, J.; Alvarez, R.; Pallares, J.; Fery, A.; de Lera, A. R.; Marsal, L. F.; Alvarez-Puebla, R. A. *Angew. Chem. Int. Ed.* **2013**, *52*, *6459*.
17. Blatchford, M. A.; Raveendran, P.; Wallen, S. L. *J. Am. Chem. Soc.* **2002**, *124*, *14818*.
18. Holka, F.; Urban, M.; Neogrády, P.; Paldus, J. *J. Chem. Phys.* **2014**, *141*, *214303*.
19. He, L.; Liu, Y.; Liu, J.; Xiong, Y.; Zheng, J.; Liu, Y.; Tang, Z. *Angew. Chem. Int. Ed.* **2013**, *52*, *3741*.
20. Shekhah, O.; Liu, J.; Fischer, R. A.; Woll, C. *Chem. Soc. Rev.* **2011**, *40*, *1081*.
21. Zhao, Y.; Kornienko, N.; Liu, Z.; Zhu, C.; Asahina, S.; Kuo, T.-R.; Bao, W.; Xie, C.; Hexemer, A.; Terasaki, O.; Yang, P.; Yaghi, O. M. *J. Am. Chem. Soc.* **2015**, *137*, *2199*.
22. Deliere, L.; Villemot, F.; Farrusseng, D.; Galarneau, A.; Topin, S.; Coasne, B. *Microporous Mesoporous Mater.* **2016**, *229*, *145*.
23. Simmons, J. M.; Wu, H.; Zhou, W.; Yildirim, T. *Energy Environ. Sci.* **2011**, *4*, *2177*.
24. Coasne, B.; Galarneau, A.; Gerardin, C.; Fajula, F.; Villemot, F. *Langmuir* **2013**, *29*, *7864*.
25. Rycenga, M.; Kim, M. H.; Camargo, P. H. C.; Cobley, C.; Li, Z.-Y.; Xia, Y. *J. Phys. Chem. A* **2009**, *113*, *3932*.
26. Lee, Y. H.; Shi, W.; Lee, H. K.; Jiang, R.; Phang, I. Y.; Cui, Y.; Isa, L.; Yang, Y.; Wang, J.; Li, S.; Ling, X. Y. *Nat. Commun.* **2015**, *6*, *6990*.
27. Besnard, M.; Cabaco, M. I.; Chavez, F. V.; Pinaud, N.; Sebastiao, P. J.; Coutinho, J. A. P.; Danten, Y. *Chem. Commun.* **2012**, *48*, *1245*.
28. Solymosi, F. *J. Mol. Catal.* **1991**, *65*, *337*.
29. Lu, Y.-H.; Yang, C.-W.; Fang, C.-K.; Ko, H.-C.; Hwang, I.-S. *Sci. Rep.* **2014**, *4*, *7189*.
30. Donnelly, S. E.; Birtcher, R. C.; Allen, C. W.; Morrison, I.; Furuya, K.; Song, M.; Mitsuishi, K.; Dahmen, U. *Science* **2002**, *296*, *507*.
31. Sheiko, S. S.; Zhou, J.; Arnold, J.; Neugebauer, D.; Matyjaszewski, K.; Tsitsilianis, C.; Tsukruk, V. V.; Carrillo, J.-M. Y.; Dobrynin, A. V.; Rubinstein, M. *Nat. Mater.* **2013**, *12*, *735*.
32. Besnard, M.; Cabaço, M. I.; Talaga, D.; Danten, Y. *J. Chem. Phys.* **2008**, *129*, *224511*.
33. Laane, J.; Dakkouri, M.; van der Veken, B.; Oberhammer, H. Structures and conformations of non-rigid molecules; Springer; Netherlands, 1993.
34. Phan-Quang, G. C.; Lee, H. K.; Ling, X. Y. *Angew. Chem. Int. Ed.* **2016**, *55*, *8304*.
35. Kuo, C.-H.; Tang, Y.; Chou, L.-Y.; Sneed, B. T.; Brodsky, C. N.; Zhao, Z.; Tsung, C.-K. *J. Am. Chem. Soc.* **2012**, *134*, *14345*.
36. Na, K.; Choi, K. M.; Yaghi, O. M.; Somorjai, G. A. *Nano Lett.* **2014**, *14*, *5979*.

TABLE OF CONTENT